Journal of Mathematical Chemistry Vol. 38, No. 2, August 2005 (© 2005)
DOI: 10.1007/s10910-005-5422-8

Flow analysis deconvolution for kinetic information reconstruction

A. Abad, S.C. Cardona, J.I. Torregrosa, F. López, and J. Navarro-Laboulais *

Technical University of Valencia–EPSA, Department of Chemical and Nuclear Engineering, Paseo Viaducto 1, 03801 Alcoy (Alicante), Spain
E-mail: jnavarla@iqn.upv.es

Received 7 March 2005; revised 22 March 2005

In this work it is proposed a methodology for the kinetic information reconstruction based on the definition of a macrotransport transfer function and a numerical regularisation method. In continuous flowing systems there could be a discrepancy, for fast enough processes, between the read measure in the detector and what actually happens in the chemical reactor. This difference is a consequence of the solute dispersion along the tube. To solve this problem we define a macrotransport transfer function from the Aris–Taylor dispersion theory which enables us a direct interpretation of the experimental data (convolution) or signal reconstruction (deconvolution). The methodology proposed consists in data processing using Tikhonov regularisation method in combination with a specific experimental procedure which allows to characterize the dispersion of the solute along the flowing system. Preliminary results for the determination of the specific area of a gas–liquid reactor are shown analysing the reaction data between the ozone and the Blue Indigotrisulfonate.

KEY WORDS: flow analysis, FIA, dispersion, ill-posed problems, signal reconstruction, reaction kinetic analysis

1. Introduction

This study is related to the interpretation and analysis of chemical kinetic data when they are collected through an experimental set-up such as the sketched in figure 1. The peristaltic pump impels the sample towards the detector which continuously records the physical magnitude that is usually related to the concentration in the reactor. For slow chemical processes, the change of the concentration in the reactor is negligible in the time interval defined by the residence time of the analyte in the tube L of figure 1. In this particular case, the measure read at the detector corresponds to the actual measure of the concentration in the reactor. This fact is well-known and it allowed the development of Flow

* Corresponding author.

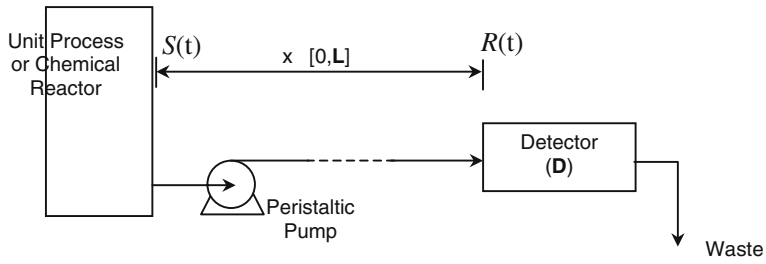

Figure 1. Experimental set-up for continuous flow analysis. When the tube radius is several orders of magnitude smaller than its length, the one-dimensional macrotransport dispersion equation describes the read at the detector. Because of the dispersion phenomenon, there is a discrepancy between the read measure, $R(t)$ and the actual measure at the inlet of the dispersion tube, $S(t)$.

Injection Analysis (FIA) techniques for the kinetic studies of chemical reactors. Moreover, for slow chemical reactions, samples from the reaction vessel can be taken out by hand in order to evaluate the concentration. But for fast kinetics this procedure is not appropriate because the measurement time could be greater or in the same order of magnitude of the exhaustion of the chemical reaction. The FIA allows a fast sample rate when optical detectors such as the UV-Vis spectrophotometers are used. The typical experimental set-up for a FIA system consists of a peristaltic pump which drives the solution to be analysed and/or the carrier solution towards the detector (see figure 1). Additional devices could be placed along the main line in order to reproduce the usual manipulation in a laboratory of analytical chemistry and to obtain the value of the concentration, i.e., heating, mixing, chemical reaction, etc.

Moreover for fast chemical processes the data acquisition rate in the detector could be increased but a more careful interpretation of data is needed. In this situation, the key concept which governs the relation between the physical measure and the concentration in the reactor is the dispersion of the analyte along the tube. In this work, we shall consider the definition of dispersion given by Brenner and Edwards as a global spatial spread of an initially inhomogeneously distributed packet of some conserved entity owing to a stochastic transport mechanism superposed upon a deterministic inhomogeneous, convective transport mechanism [1]. From this starting point of view and assuming the asymptotic conditions defined by Taylor [2,3] and Aris [4], the Taylor–Aris convection–diffusion macrotransport equation will be considered as a valid hypothesis in order to describe the dispersion of the analyte along the dispersion tube in figure 1.

$$\frac{\partial \bar{C}}{\partial t} = \bar{D}^* \frac{\partial^2 \bar{C}}{\partial z^2} - \bar{U}^* \frac{\partial \bar{C}}{\partial z}. \tag{1}$$

The notation of Brenner and Edwards [1] is used here. $\bar{C}$ is the area-average concentration, $\bar{D}^*$ the macroscale convection dispersivity dyadic, $\bar{U}^*$ the area-average axial velocity of the fluid, z the axial coordinate and t the time.

Accepting these hypothesis, the aim of this work is to define a transfer function for the dispersion phenomenon allowing the semi-empirical characterisation of macrotransport processes and its experimental validation. The transfer function formalism allows the treatment of complex systems that cannot be approached anyway else. Consider, for instance, a system composed by a connected series of CSTR with different residence times in which a solute is injected initially at the beginning of the line. The existence of different initial and boundary conditions along the line hinders the evaluation of an equation describing the evolution of the concentration at the end of such a system. In addition, this formalism does not necessarily implies solving the set of partial differential equations that describes the system because empirical transfer functions could be used instead. Once the transfer function of the system has been characterised analysing the response to well-known input signals, the deconvolution of the experimental responses can be envisaged if a stable algorithm is available. The contribution of this work deals with the use of the transfer function formalism for describing the dispersion of a solute through a cylindrical tube in the Poiseuille regime and the description of a stable algorithm which allows the reconstruction of any arbitrary input signal. Although the transfer function formalism is widely used in control theory and normally by chemical engineers, no examples about the use of this formalism for kinetic information reconstruction have been found in the literature. A partial description of this approach has previously been proposed elsewhere by the authors [5,6]. A complete description of the methodology is proposed in this paper.

This paper is structured as follows. First, the transfer function is derived from equation (1). Then, the use of this transfer function is shown for different physicochemical processes and their respective concentration–time expressions are derived. Finally, the deconvolution of dispersion data is shown as an extension of the transfer function formalism and a new procedure for the analysis of kinetic data is proposed.

2. Definition of the macrotransport transfer function

A transfer function relates the response and the perturbation of a linear dynamical system [7,8]. Any physical system that can be described by a linear differential equation with all their values initially set to zero, can be modelled through a transfer function. If we suppose a system which is perturbed by a signal $S(t)$, it will respond to this perturbation giving the response $R(t)$. Considering the convolution theorem, both signals $S(t)$ and $R(t)$ could be related through the transfer function of the system. Then, in this work the concentration in the

reactor is visualized as a perturbation applied at the inlet of the tube of length L and moving towards the detector.

The dispersivity constant, $\overline{D}^*$, and the area-average velocity, $\overline{U}^*$, defined in equation (1) are two phenomenological coefficients which are related to local and global magnitudes of the system. It is important from an experimental point of view to conserve this feature and then, it is advisable to use a transfer function with two adjustable parameters. This point also is justified in the theoretical framework of macrotransport processes. If the phenomenological parameters $\overline{D}^*$ and $\overline{U}^*$ collect the local information about the physicochemical processes as a result of the simplifications of microtransport equations, less parameters could imply a significant loss of information. Once the parameters have been experimentally obtained, their behaviour should be checked in order to validate the transfer function and the model.

The transfer function is derived from the partial differential equation (1) in the bounded space $0 < z < L$. The transfer function of a linear system with initial conditions set to zero (in our case $\bar{C}(z, t) = 0 \quad \forall t < 0,\ z \in [0, L]$) is defined as the ratio between the system output and the perturbation input in the Laplace domain. Then, considering that at the beginning of the dispersion tube an arbitrary perturbation $\bar{C}(0, t)$ is applied and that the concentration at the output of the tube should be bounded, from equation (1) the transfer function for the dispersion phenomenon, $h(p)$, is deduced:

$$h(p) = \frac{c(L, p)}{c(0, p)} = \exp\left[\alpha\ \beta - \alpha\ \left(p + \beta^2\right)^{1/2}\right], \tag{2}$$

where $c(\cdot, p)$ is the Laplace transform of the area-average concentration and α and β the new semi-empirical dispersion parameters defined as:

$$\alpha = \frac{L}{(\overline{D}^*)^{1/2}},$$
$$\beta = \frac{\bar{U}^*}{2\ (\overline{D}^*)^{1/2}}. \tag{3}$$

We must have in mind that the original problem was to obtain information of the chemical reactor or process that is connected with a detector as is shown in figure 1. The equation (2) relates the measured response in the detector with the perturbation or the variation of concentration at the input of the tube. It is noticeable here that this transfer function is valid only when no chemical reaction happens in the dispersion tube. This case is achievable only when fast reactions occur just in the reactor and the reaction rate is negligible at the tube entrance, e.g., when one of the reactants is exhausted in the first section of the tube. This case will be later exemplified with a fast gas–liquid chemical reaction.

Once the transfer function is derived, two approaches are used to obtain information of the system under study. The first one is based on the application

of the convolution theorem and the Laplace inversion of the result. This method has the advantage that it is easy to carry out when easy perturbations or kinetics are considered, but that implies an *a priori* knowledge of the process in the reactor. This methodology enable us to deduce the response in the detector having an analytical function that depends on the dispersion parameters α and β and they are evaluated by non-linear regression. The second methodology is a more numerical method based on the deconvolution or unfolding of the signal measured in the detector. The perturbation is obtained solving the convolution integral once the measured response and the transfer function are combined to solve a linear system of equations. In this case, none or little knowledge about the perturbation is needed in order to unfold the response of the system. Thus, before showing the experimental results, let's explain the theoretical foundations of both methods with some detail.

2.1. Laplace inversion: analytical convolution

Let $s(p)$ and $r(p)$ the Laplace transform of the signal, $S(t)$, and the response, $R(t)$, of the system, respectively. Using the convolution theorem, both Laplace functions are related through the transfer function of the dispersion system (equation (2)) $r(p) = h(p) \cdot s(p)$. Thus, the temporal response observed in the detector is obtained by Laplace inversion of the precedent product. Let's consider two perturbations which are easy to carry out in the laboratory in order to characterise the dispersion phenomena: (i) a concentration step, and (ii) a concentration pulse of duration τ.

In the first situation we have at $z = 0$:

$$S(t) = C_0 \cdot U(t), \tag{4}$$

where $U(t)$ is the unitary step or Heaviside function. The convolution theorem allows the evaluation of the response of the detector:

$$\overline{C}(L,t) = \int_0^t H(\theta) \cdot C_0 \, \mathrm{d}\theta = C_0 \frac{\alpha}{2\pi^{1/2}} \int_0^t \theta^{-3/2} \exp\left[-\frac{(\alpha - 2\beta\theta)^2}{4\theta}\right] \mathrm{d}\theta, \tag{5}$$

where $H(t)$ is the inverse Laplace transform of equation (2) and θ the integration variable. Defining two new variables $y = (\alpha + 2\beta\theta)/2\theta^{1/2}$ and $x = (\alpha - 2\beta\theta)/2\theta^{1/2}$ equation (5) can be rewritten in a more convenient way as:

$$\overline{C}(L,t) = C_0 \cdot F_S(t) = C_0 \cdot \frac{1}{2}\left\{\mathrm{Erfc}\left(\frac{\alpha - 2\beta t}{2t^{1/2}}\right) + \exp(2\alpha\beta)\ \mathrm{Erfc}\left(\frac{\alpha + 2\beta t}{2t^{1/2}}\right)\right\}, \tag{6}$$

where $\mathrm{Erfc}(x)$ is the complementary error function [9]. For convenience let us call the term in brackets, $F_S(t)$, which represents the response of a unitary step

perturbation for a pure dispersion process. There are accurate and fast algorithms which calculate the error function in equation (6) more efficiently than the particular integral defined in (5). Thus, this last function is advantageous in order to calculate the parameters α and β from experimental data and was used to obtain the results shown below. There is not an easy physical interpretation of parameters α and β from dimensional analysis, but from a phenomenological point of view the parameter α is related to the time lag of the signal, increasing this magnitude as α does, and the parameter β is related to the dispersion of the concentration in the tube, decreasing the slope in the inflexion point and the overall curve width as β increases. In the experimental section a methodology for the calculation of α and β based on residence-time distribution functions will be suggested.

The second kind of perturbation proposed is a concentration pulse of duration τ. In this case, the applied perturbation in $z = 0$ can be written as:

$$S(t) = C_0 \{U(t) - U(t - \tau)\}, \tag{7}$$

where τ is the duration of the pulse. Considering the definition of $F_S(t)$ (equation (6)), after the Laplace inversion, it could be demonstrated that the response of the system is

$$\bar{C}(L, t) = C_0 \{F_S(t) - U(t - \tau) \cdot F_S(t - \tau)\}. \tag{8}$$

For small values of τ, this function shows a maximum which generally is used in analytical chemistry as the measured magnitude in FIA technique. In this context, the ratio between the input concentration and the concentration at the maximum is called 'dispersion', which depends on the liquid flow, the tube length and the dispersion coefficients in a complex way [10,11] .

Summarising, it is possible the evaluation of the response of the detector in figure 1 when some kind of known perturbation is applied at the beginning of the dispersion tube by using the transfer function equation (2) together with the Laplace inversion. That implies that the time-concentration evolution in the reactor should be known before the experiment and that the Laplace inversion should be performed. Because this is a significant limitation for the study of real or complex systems, an alternative method based on numerical deconvolution of the measured response of the system is proposed.

2.2. *Numerical deconvolution*

This method attempts to obtain a numerical approximation to the solution of the convolution equation:

$$R(t) = \int_0^t H(t - \theta)\ S(\theta)\ \mathrm{d}\theta. \tag{9}$$

If $R(t)$ and $H(t)$ are known, equation (9) is a Volterra integral equation of the second kind [12]. Let's consider that the values of the perturbation $S(t)$ are only available at some discrete values of t. Then, using the Heaviside function, $S(t)$ can be written as a linear combination of this unitary function:

$$S(t_k) = S_0 + \sum_{i=1}^{k-1} \Delta S_i \; U(t_k - t_i), \quad k = 1, \ldots, N, \tag{10}$$

where S_0 is the initial value of the perturbation and ΔS_i are constants that should be evaluated. Substituting equation (10) in (9), the response of the system at time t_k is

$$R(t_k) = S_0 \; F_S(t_k) + \sum_{i=1}^{k-1} \Delta S_i \; F_S(t_k - t_i), \tag{11}$$

where $F_S(t)$ is the response of a unit-step perturbation (see equation (6)). The only unknowns in equation (11) are the constants ΔS_i which can be obtained solving the set of linear equations defined by the discrete representation of the integral (9):

$$\begin{pmatrix} R(t_1) \\ R(t_2) \\ R(t_3) \\ \vdots \\ R(t_N) \end{pmatrix} = \begin{pmatrix} F_S(t_1) & 0 & 0 & \cdots & 0 \\ F_S(t_2) & F_S(t_2 - t_1) & 0 & \cdots & 0 \\ F_S(t_3) & F_S(t_3 - t_1) & F_S(t_3 - t_2) & \cdots & 0 \\ \vdots & \vdots & \vdots & \cdots & \vdots \\ F_S(t_N) & F_S(t_N - t_1) & F_S(t_N - t_2) & \cdots & F_S(t_N - t_{N-1}) \end{pmatrix} \begin{pmatrix} S_0 \\ \Delta S_1 \\ \Delta S_2 \\ \vdots \\ \Delta S_{N-1} \end{pmatrix}, \tag{12}$$

which can be written in a more compact form as $\mathbf{R} = \mathbf{F} \cdot \mathbf{\Delta S}$. The solution of the system (12) is an apparently straightforward matter and looks easy using a simple backsubstitution algorithm. Nevertheless, the matrix $\mathbf{F}$ is nearly singular and then, its inversion leads to an unstable operation resulting in a rapidly oscillating solution because of the experimental error in the measured response, $R(t)$. This kind of problems are known as discrete *ill-posed* problems which are frequent in experimental physics where the perturbation and the response are related to convolution integrals such as equation (9) or Fredholm integral equation of the first kind, i.e., optical image reconstruction, acoustic source reconstruction [13], the characterisation of detectors used in high-energy physics [14] or the determination of probability distribution functions of relaxing times in electrochemistry [15,16].

The primary difficulty with the discrete ill-posed problems is that they are essentially undetermined and unstable. Thus, further information about the desired solution should be included to single out and stabilise a useful solution. This can be achieved by using *regularisation methods* such as the truncated singular value decomposition (TSVD) [6], the damped singular value decomposition

(DSVD) [14], the maximum entropy method (MEM) [17] and the most common and well-known *Tikhonov regularisation method* which has been used in this work [18,19]. The idea here is to obtain a solution $\mathbf{\Delta S}_\lambda$, which minimises a weighted combination of the residual norm, $\|\mathbf{F}\cdot\mathbf{\Delta S}-\mathbf{R}\|_2^2$ (equivalent to solving a least squares problem) with the side constraint norm $\|\mathbf{L}(\mathbf{\Delta S}-\mathbf{\Delta S}^*)\|_2^2$ as:

$$\mathbf{\Delta S}_\lambda = \min\left\{\left\|\mathbf{F}\cdot\mathbf{\Delta}\boldsymbol{S}-\mathbf{R}\right\|_2^2+\lambda^2\left\|\mathbf{L}(\mathbf{\Delta S}-\mathbf{\Delta}\boldsymbol{S}^*)\right\|_2^2\right\}, \tag{13}$$

where λ is the regularisation parameter and controls how much weight is given to minimisation of the residual norm related to the side constraint norm. The regularisation parameter controls the properties of the regularised solution, so it should be computed carefully with some numerical method. $\mathbf{L}$ is typically the identity or a nth derivative matrix which bias or smoothes the rapid oscillations of the solution and $\mathbf{\Delta S}^*$ is an initial estimate or hypothesis about the solution which could only be known in some particular cases.

A feasible solution of (13) is attained performing the singular value decomposition (SVD) of the dispersion matrix $\mathbf{F}$. A SVD of a real matrix is a factorisation of the form:

$$\mathbf{F}=\mathbf{U}\cdot\mathbf{W}\cdot\mathbf{V}^{\mathbf{T}}, \tag{14}$$

where $\mathbf{U}$ and $\mathbf{V}$ are both orthogonal matrices and $\mathbf{W}$ is a diagonal matrix with non-negative or zero diagonal elements, w_i, appearing in decreasing order. This kind of decomposition is unconstrained to how singular the matrix $\mathbf{F}$ is and can always be done. In our case, the dispersion matrix is square and then, $\mathbf{U}$, $\mathbf{W}$ and $\mathbf{V}$ are all square matrices. The direct solution of (12) implies the inversion of (14). Because $\mathbf{U}$ and $\mathbf{V}$ are orthogonal matrices and $\mathbf{W}$ is a diagonal matrix, we have:

$$\mathbf{F}^{-\mathbf{1}}=\mathbf{V}\cdot\mathbf{W}^{-1}\cdot\mathbf{U}^{\mathbf{T}} \tag{15}$$

and then, the solution $\mathbf{\Delta S}$ of (13) is:

$$\mathbf{\Delta S}=\mathbf{V}\cdot\left[\operatorname{diag}\left(\frac{1}{w_i}\right)\right]\cdot\left(\mathbf{U}^{\mathbf{T}}\cdot\mathbf{R}\right)=\sum_{i=1}^{N}\mathbf{v}_i\frac{1}{w_i}\left(\mathbf{u}_i^T\cdot\mathbf{R}\right), \tag{16}$$

where w_i are the singular values while $\mathbf{v}_i$ and $\mathbf{u}_i$ are the singular vectors of the matrix $\mathbf{F}$, respectively. Equation (16) shows that this solution is dominated by the smallest singular values of $\mathbf{F}$ and consequently the result seems completely random.

The purpose of regularisation is to filter out these dominant contributions introducing in equation (16) a series of filter factors, f_i, which definition depends on the particular regularisation method. The main property of f_i is that it tends to zero as w_i decreases removing then these contributions. Considering that

the matrix $\mathbf{L}$ in (13) is square and invertible, let us define the new quantities $\bar{\mathbf{F}} = \mathbf{F} \cdot \mathbf{L}^{-1}$, $\bar{\mathbf{R}} = \mathbf{R} \cdot \mathbf{L}^{-1}$ and $\boldsymbol{\Delta}\bar{\mathbf{S}}^* = \mathbf{L} \cdot \boldsymbol{\Delta}\mathbf{S}^*$. The regularised solution of the equation (13) using Tikhonov's regularisation method is given by:

$$\left(\boldsymbol{\Delta}\overline{S}_\lambda\right)_i = \frac{w_i \cdot (\overline{\mathbf{U}}^T \cdot \overline{\mathbf{R}})_i + \lambda^2 \cdot (\overline{\mathbf{V}}^T \cdot \boldsymbol{\Delta}\overline{S}^*)_i}{w_i^2 + \lambda^2}, \tag{17}$$

where the bar over the singular values and vectors refers to the SVD of $\bar{\mathbf{F}}$. The regularised solution (17) is then transformed back to the original regularised solution (13) by $\boldsymbol{\Delta}\mathbf{S}_\lambda = \mathbf{L}^{-1} \cdot \boldsymbol{\Delta}\bar{S}_\lambda$.

In conclusion, the numerical deconvolution of the measure given by the detector of the experimental set-up system depicted in figure 1 it is possible when solving equation (17). The algorithm needs the values of the dispersion parameters α and β in order to evaluate the matrix $\mathbf{F}$. These parameters should be determined before the deconvolution in a set of independent experiments. Then, the matrices $\mathbf{F}$, $\mathbf{L}$ and the vector $\boldsymbol{\Delta}\mathbf{S}^*$ are initialised, equation (17) is evaluated and finally the original perturbation of the system is reconstructed applying equation (10).

3. Experimental

The validity of the transfer function approach for studying dispersion phenomena has been checked with two kinds of experiments. First, a simple step or pulse of known concentration has been recorded and the dispersion parameters have been calculated for different flow rates. These experiments enable us to check the validity of the equations developed in the section 2.1 from the transfer function and the study of the calculated dispersion parameters. The second kind of experiments were designed in order to explore the possibilities of the numerical deconvolution method described in section 2.2. Hence, a complex enough chemical reacting system was preferred for this study where the kinetic data were not accessible otherwise. A fast gas–liquid chemical reaction, i.e., ozone + indigotrisulphonate, it is a good candidate because is easy to carry out in the laboratory and the process depends on physical and chemical magnitudes.

An experimental set-up such as the figure 1 based on a peristaltic pump (Gilson Minipuls 3) generally used in FIA experiments has been used. The reactor and the detector were connected with Teflon tubes greater than 2.0 m length and 0.8 mm of inner diameter. The generation of the steps and pulses was done with a three-way injection valve (Rheodyne model 5020) allowing the switching between distilled water and the solution under study. This injection valve was placed between the pump and the dispersion tube. The sample flowed towards a Suprasil® quartz flow cell (Hellma Mod. 178.710-QS) placed in a UV–vis spectrophotometer (Unicam Helios γ).

Tartrazine (Acid Yellow 23, CI 19140, CAS 1934-21-0) provided by Color-Center S.A. was used for dispersion experiments. This substance shows an absorbance maximum at 427 nm. On the other hand, Blue Indigo solutions were prepared from the substance supplied by Riedel-de Haën (5,5′,7-Indigotrisulfonic acid tripotassium salt, CAS 28606-01-1). The maximum absorbance of these solutions is found at 600 nm. All chemicals used in this study were of analytical degree. Millipore Elix 3 deionised water was used to prepare all solutions in the experiments.

A bubble-column reactor of 0.5 L and 60 mm of inner diameter was used for gas–liquid reactions. Ozone was generated by passing pure oxygen (Carburos Metálicos, Clase 2) through an electrical discharge 300 W ozone generator (Multiozono model DC-OM.12), with a maximum working pressure of 4 bar and a maximum ozone production of 12 g/h O_3. The ozone concentration in the gas phase measured with an Anseros Ozomat GM 6000 RTI Ozone Analyzer, ensuring that it remains constant along the experiment. The temperature of the reactor was maintained constant with a Selecta Frigiterm Thermostat.

The dispersion parameters α and β and their confidence intervals were calculated using the non-linear regression routines defined in the software Mathematica® based on the Levenberg–Marquardt algorithm. Alternatively, these magnitudes can be calculated from the nth moments of the concentration–time curve. Let's suppose that $C(t)$ is the recorded experimental response of the dispersion system to a step perturbation, given by equation (6). Thus, the dispersion parameters α and β are given by:

$$\alpha = \left(\frac{2\,\mu_1^3}{\mu_2 - \mu_1^2} \right)^{1/2}, \tag{18.a}$$

$$\beta = \left(\frac{\mu_1}{2\left(\mu_2 - \mu_1^2\right)} \right)^{1/2}, \tag{18.b}$$

where μ_i is the ith moment of the curve $C'(t) = \mathrm{d}C(t)/\mathrm{d}t$ given by:

$$\mu_i = \frac{1}{C(t \to \infty)} \int_0^\infty t^i\, C'(t)\, \mathrm{d}t. \tag{19}$$

4. Results

In a first series of experiments, Tartrazine pulses with different duration have been generated switching a colorant solution into the carrier through the detector (see figure 1). Pulses of 10–80 s in steps of 10 s have been generated at constant flow velocity of 3.42 cm/s in a dispersion tube of 1.75 m. Because of the linear relationship between concentration and absorbance, this measured magnitude has been directly fitted to equation (8) in order to obtain the dispersion

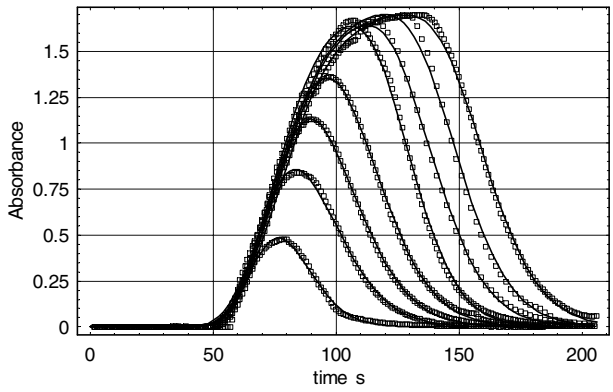

Figure 2. Tartrazine pulse experiments for different pulse duration. The curves are the best fit to equation (8) with τ as a free fitting parameter. From left to right, the pulse duration ranged from 10 to 80 s in steps of 10 s. [Tartrazine] $= 8.4410^{-5}$ M; Tube length, $L = 1.75$ m; flow velocity, $u = 3.42\,\mathrm{cm\,s^{-1}}$; $T = 293$ K.

parameters α and β. Two strategies have been designed to check the equation adequacy and the fitting accuracy. First, the pulse duration was set constant in equation (8) and equal to its nominal value. In a second program, the duration pulse, τ, was considered also as a fitting parameter and then, the calculated one was compared with its nominal value. The results obtained following this methodology are plotted in figure 2.

The fitting parameters of both methodologies are collected on figure 3. The confidence interval of each fit for every parameter is smaller than the size of the symbol. Open symbols correspond to the fit with fixed τ, and the crossed ones, to the free τ. These results show that the dispersion parameters α and β have not significant differences using both methodologies. Conversely, the constant C_0, which here means the maximum absorbance of the solution, has a significant difference for pulse duration below 40 s, but converges to the same solution for higher times. This difference is also corroborated when the calculated pulse duration is plotted against its nominal value. Figure 4 shows the best fit values for τ together with the line through the origin with unit slope. For $\tau \leqslant 40$ s the calculated values deviate from its nominal one and their error is considerable, so they should be considered undetermined with this procedure. For small values of τ, the applied perturbation at the inlet of the dispersion tube looks like an impulse perturbation. In this case, the measured response differs significantly from the equation (8) and depends basically on α and β but not on τ. Then, for short pulses the dispersion is the main phenomenon governing the response of the system. In other words, for short pulses the dispersion phenomenon masks or suppresses information about the perturbation at the tube inlet.

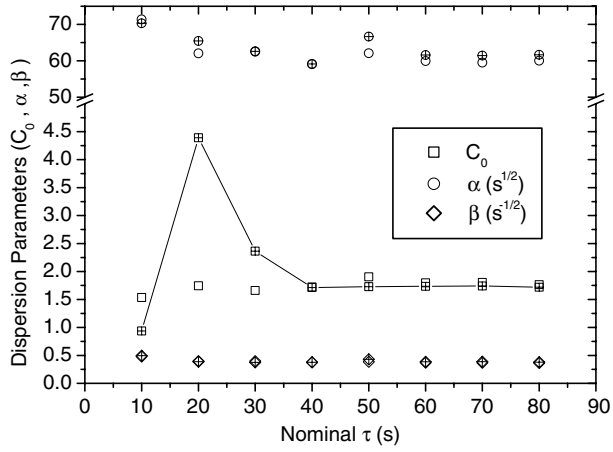

Figure 3. Calculated dispersion parameters from data of figure 2. The crossed symbols correspond to the free-τ strategy while the open ones are the result of fixing τ to its nominal value. The concentration, C_0, is calculated in absorbance units. The nominal maximum absorbance is 2.17.

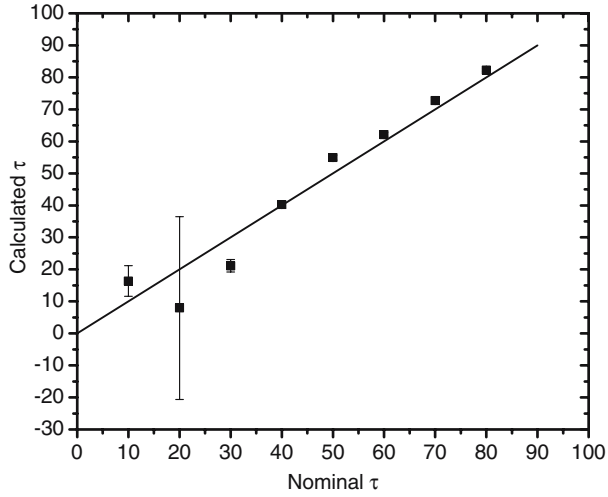

Figure 4. Calculated τ versus its nominal value. The line is a guide to the eye and has a slope of 1. For pulses greater than 40 s the calculated value of τ does not differ from its nominal value. For lower times, the solute dispersion masks information about the perturbation at the tube inlet and results in an inaccurate determination of the pulse duration.

Considering the Aris–Taylor macrotransport equation for the dispersivity constant, the determination of the diffusion coefficient is a straightforward matter [1,20]:

$$\overline{D}^* = D + \frac{\left(\overline{U}^*\right)^2 R_0^2}{48\ D}, \tag{20}$$

where R_0 is the inner radius of the dispersion tube and D the molecular diffusivity of the solute. Considering the dispersion parameter β, the molecular diffusivity of the solute can be calculated from

$$D = \frac{1}{12} R_0^2 \beta^2. \tag{21}$$

From data plotted in figure 3, considering that the inner radius of the dispersion tube is 0.04 cm and using an average value of $\beta = 0.39 \pm 0.03 s^{-1/2}$, the Tartrazine diffusivity is $2.03 \times 10^{-9} m^2 s^{-1}$. This value is similar to previously reported [5].

A second series of experiments were designed in order to check the transfer function (2) using the procedure described in section 2.2. In this case the reaction between ozone gas and Blue Indigo was investigated using the apparatus depicted in figure 1. Initially, the dispersion tube was filled up with distilled water ensuring the zero-concentration initial condition. The Blue Indigo solution was then placed in the reactor and the peristaltic pump was switched on. The absorbance of the solution was continuously recorded until its value reached a plateau corresponding to the dye solution absorbance. Maintaining the solution flowing through the tube, a stream of ozone gas was bubbled in the reactor at time t_0 and the colour depletion was recorded with the spectrophotometer. A typical experiment is plotted in figure 5. The arrow in the figure indicates the instant at which the ozone begins to bubble in the reactor.

This experimental procedure allow us to consider the data divided in two zones. The first one, for $t < t_0$, should be used for the determination of the dispersion parameters. Because flow conditions were not modified in the second part of the experiment, it would not be unreasonable to consider that the previously calculated α and β remain valid. Therefore, with the experimental data of this first zone the matrix $\mathbf{F}$ in equation (12) is able to be built. The data of the second zone ($t > t_0$) will be used for deconvolution and to reconstruct what happened in the reactor.

Let's recall that deconvolution implies the calculation of the coefficients $\boldsymbol{\Delta}\bar{\mathbf{S}}_\lambda$ given by equation (17) and the reconstruction of the perturbation using equation (10). The algorithm for numerical deconvolution implies first the calculation of the matrix $\mathbf{F}$ as was described using the dispersion parameters. Then, this matrix is decomposed using a SVD algorithm in order to obtain the matrices in equation (14). Note that in equation (17) the initial estimate of the solution $\boldsymbol{\Delta}\bar{\mathbf{S}}^*$ is present. This quantity should be considered as a vector which contains some initial hypothesis about the solution and could not be exhaustive in the sense that partial information is enough to improve some approximate solution. In order to prove this, different hypothesis about the solution were tested. Some have a theoretical justification, but others have been used just to check the given regularised solution.

Because the chemical process we are studying is a fast gas–liquid chemical reaction, we will consider here the two-film theory in order to elaborate the

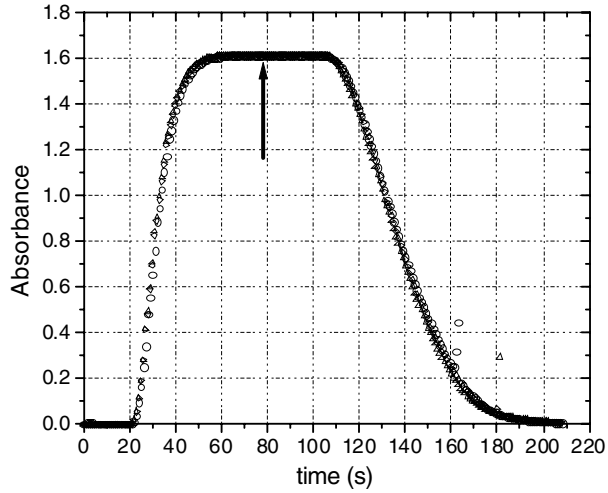

Figure 5. Typical measured response in a dispersion+gas–liquid reaction experiment. Initially the reactor is full of Blue Indigo solution and the dispersion tube is full of water. A step-dispersion experiment is performed to obtain the dispersion coefficients α and β. Once reached the absorbance plateau, an ozone-gas stream is bubbled through the solution. After the ozone injection, instant marked with the arrow, the colour dye depletion follows. $[BI]_0 = 9.7 \times 10^{-5}$ M. $[O_3]_{g0} = 3.3\,g\,m^{-3}$; $T = 293$ K; Tube length, $L = 3.14$ m; flow velocity, $u = 11.1\,cm\,s^{-1}$; gas flow $q_g = 109\,L\,h^{-1}$; mean dispersion parameters: $\alpha = 37.77\,s^{1/2}$, $\beta = 0.592\,s^{-1/2}$.

hypothesis $\mathbf{\Delta}\bar{\mathbf{S}}^*$. A complete description of physicochemical processes involved in gas–liquid reactions is beyond the scope of this paper, so we will outline a simple model which complete description is available elsewhere [21–24]. Let's consider perfect mixed flow for liquid and gas phases in the reactor and a first order reaction for ozone and Blue Indigo. If pseudo-first-order fast kinetic regime holds, the dye concentration evolution in the bulk solution can be approached by

$$C^{1/2} = C_0^{1/2} - A \cdot t, \tag{22}$$

where,

$$A = \frac{z \cdot a \cdot [O_3]\,RT}{He} k_2^{1/2}\ D_{O_3}^{1/2}, \tag{23}$$

z is the stoichiometric coefficient between ozone and the Blue Indigo, a the gas–liquid specific interfacial area (m^{-1}), $[O_3]$ the ozone gas concentration ($mol\,L^{-1}$), He the Henry constant (atm M^{-1}), k_2 the second-order rate constant ($M^{-1}\,s^{-1}$) and D_{O_3} the ozone diffusion coefficient ($m^2\,s^{-1}$). In order to apply the fast kinetic regime (FKR) equation the condition $Ha > 3$ must also be satisfied [24], where Ha is the Hatta number.

From equation (22) it can be deduced that at initial stages of the reaction, the dye concentration in the reactor is linear with time. This behaviour has

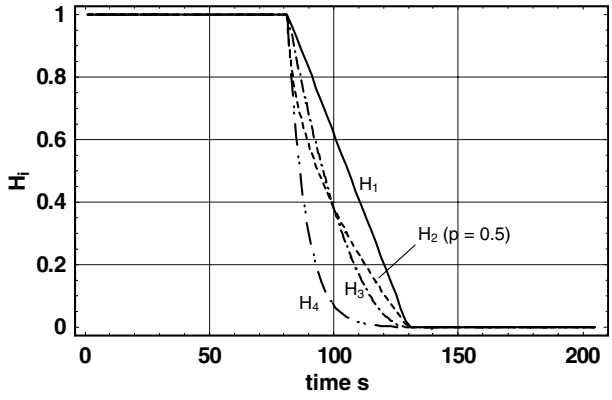

Figure 6. Initial hypothesis used in deconvolution. These functions have been used as initial estimate of the solution, $\Delta\overline{S}^*$, in equation (17) and the notation corresponds to equation (24a–e).

also been observed by solving numerically the complete set of partial differential equations describing this kind of systems [22,25]. This fact is enough to elaborate the hypothesis used for the data deconvolution. Let's suppose the following hypothesis for the evolution of the dye concentration in the reactor:

$$H_0(t) = 0, \tag{24.a}$$

$$H_1(t) = a_0 - a_1\, t, \tag{24.b}$$

$$H_2(t) = a_0 - a_1\, t^p, \tag{24.c}$$

$$H_3(t) = (a_0 - a_1\, t)^2, \tag{24.d}$$

$$H_4(t) = a_0\, \mathrm{e}^{-a_1\, t}. \tag{24.e}$$

Note that all the above equations are continuously decreasing functions. Equation (24.a) is the null-hypothesis, that is, no hypothesis about the solution is done. Equations (24.b)–(24.d) are linear or quasi-linear functions. In this case, the concentration equals to zero at some value of $t = t_c$. For higher times, the concentration will be considered null. Last equation (24.e) is an exponential decay which has only been considered for comparison purposes. All the functions have been plotted in figure 6.

Hence, $\Delta\overline{\mathbf{S}}^*$ is calculated from equations (24) and the regularised solution (17) could be determined. As was described in section 2.2, the regularised solution depends on the regularisation parameter λ, defined in equation (13), which controls the weight between the least square solution of $\mathbf{\Delta S}$ and its discrepancy with some hypothesis about this solution, $\mathbf{\Delta S}^*$. Different methodologies have been proposed for calculating the optimal value of λ [18]. The method used in this work was based on the determination of λ which maximises the curvature of the *L-curve*, a parametric plot of the residual norm $\|\mathbf{F}\cdot\mathbf{\Delta S} - \mathbf{R}\|^2$ against the side constraint norm $\|\mathbf{L}(\mathbf{\Delta S} - \mathbf{\Delta S}^*)\|^2$ as a function of λ [26].

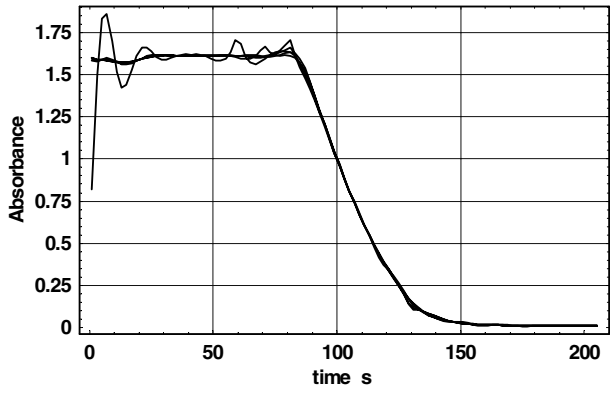

Figure 7. Effect of the initial hypothesis $\Delta\overline{S}^{*}$ on data deconvolution. The same experimental data set was considered for deconvolution using different hypothesis (see equations (24a–e)). The same deconvolved data are obtained independently of the hypothesis done about the solution. The zero hypothesis, H_0, gives an oscillatory solution which is suppressed including some additional information about the solution.

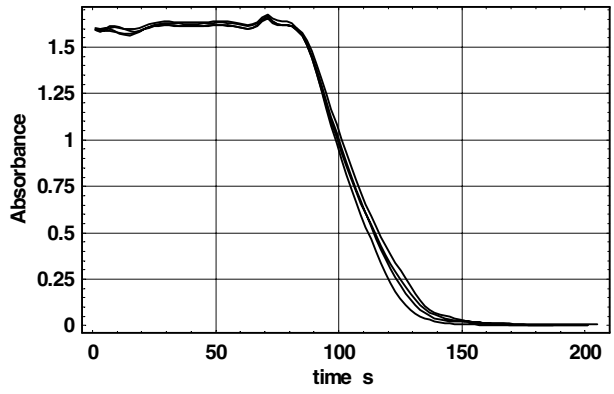

Figure 8. Deconvolution of experimental runs shown in figure 5. Note that the calculation has been carried out using the raw measured absorbance. $[BI]_0 = 9.7\times10^{-5}$ M. $[O_3]_{g0} = 3.3\,g\,m^{-3}$; $T = 293$ K; Tube length, $L = 3.14$ m; flow velocity, $u = 11.1\,cm\,s^{-1}$; gas flow $q_g = 109\,Lh^{-1}$ Hypothesis: Fast Kinetic Regime (see equation 24.d).

Once the optimal value of the regularisation parameter is obtained, the regularised solution $\Delta\mathbf{S}$ is calculated. This solution is then used with equation (10) in order to recover the perturbation at the reactor. The deconvolution of experimental data shown in figure 5 has been plotted in figures 7 and 8. In figure 7 the effect of the different hypothesis has been studied for the same set of experimental data but different equations (24). There are no significant differences in the regularised solution when this equation is changed. The only relevant information given at the algorithm is that the solution should look like that represented in figure 6. Then, we can conclude that a change in the initial

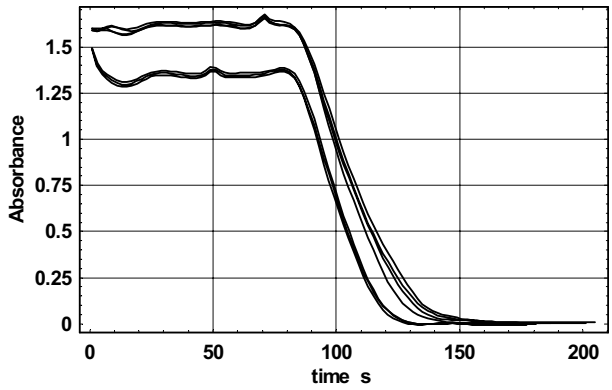

Figure 9. Deconvolution of ozone + Blue-Indigo reaction at different initial dye concentration. The calculated solution is independent of the hypothesis too. The difference between the curves heights has been detected without any change in $\mathbf{\Delta}\overline{\mathbf{S}}^{*}$.

estimate $\mathbf{\Delta S}^{*}$ does not change significantly the calculated regularised solution, and consequently, there is no reason to argue that this solution is the result of some mathematical artifact introduced by equations (24). In fact, using the null-hypothesis (equation (24.a)) the calculated solution shows the same dye depletion that the obtained with the other hypotheses, but also shows an oscillating behaviour before the ozonation which is removed when equations (24.b)–(24.e) are used.

Considering that equations (22) and (23) describe the physicochemical processes occurring in our gas–liquid system, it is then reasonable to adopt the equation (24.d) as the most feasible hypothesis for further data calculations. Changing this function will not have a significant change in the result as it was previously demonstrated, but it is preferable to work within a well-known theoretical framework. Thus, from here, all the calculations shown have been carried out using equation (24.d). The preliminary results showed next pretend to illustrate the application of flow analysis deconvolution to the study of gas–liquid reactions. Hence, only few experimental conditions were modified to observe the effect on the deconvolution, but always bearing in mind that a more detailed analysis of the reaction of ozone and the Blue Indigo will be needed in the future. In figure 8 the deconvolution of different experimental runs has been plotted. The observed differences between each run is caused by statistical fluctuations instead of modifications in the experimental conditions. All the experiments were carried out at 20°C.

Figure 9 shows the flow analysis deconvolution of two series of experiments carried out at different initial dye concentration. The maximum absorbance of the first series is around 1.6 while the second is 1.4. The importance of these curves lies on the fact that all were calculated using the same initial estimate of

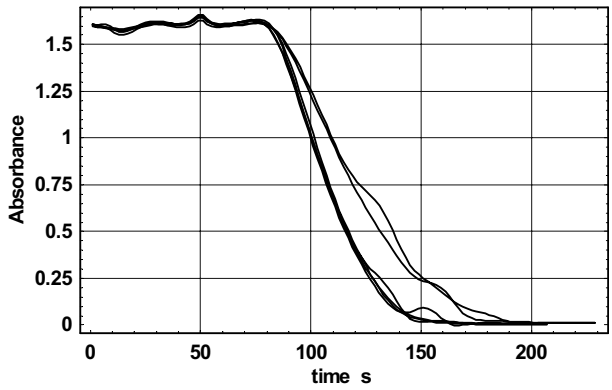

Figure 10. Effect of the ozone-gas concentration on kinetics. The deconvolution has been carried out using the same hypothesis in both series. The upper curve was obtained with $[O_3]_{g0} = 1.5\,g\,m^{-3}$ and the lower with $[O_3]_{g0} = 3.3\,g\ m^{-3}$.

the solution (equation (24.d)). Therefore, the deconvolution is sensible to experimental conditions and independent of the details of hypothesis done about the solution. It is important to confirm that equation (24) does not introduce a bias in the regularised solution if we want to use this methodology for the study of dynamic systems.

Finally, in figure 10 two series with different ozone concentration in the gas phase are shown. Let's interpret the curves considering equation (22). An increase of the ozone in the gas phase, $[O_3]$, implies an increase of the slope of the curve of the dye concentration. The ozone concentration in these series was 3.3 and $1.5\,g\,m^{-3}$, respectively. Thus, the curves shape agree with their expected behaviour.

These data allow the calculation of the specific interfacial area, a. After the correction of the time scale with the time at which the ozone starts to bubble in the reactor, the zone of interest for the study of the gas–liquid reaction phenomena is bounded. Figure 11 shows the Blue Indigo depletion which is almost completed in two minutes. The absorbance units have been maintained for simplicity, instead their conversion to concentration. Note now that FKR model (equation (22)) cuts the temporal axis at some time t_c and the function is zero for times greater than this value. Then, the fitting function

$$f(t) = \begin{cases} B^2\left(1 - \frac{t}{t_c}\right)^2, & t < t_c, \\ 0, & t \geqslant t_c \end{cases} \tag{25}$$

is defined to obtain the quantitative information of the deconvolution data. Equation (25) has two fitting parameters, B which is related to the initial dye concentration, and t_c the time at which the curve cuts the t-axis related to the previously defined constant A (see equation (23)). The results are collected on

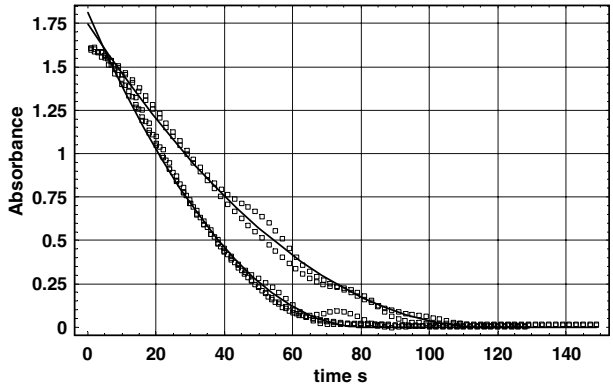

Figure 11. Analysis of the kinetic data of the reaction between the Blue Indigo and the ozone after the deconvolution and time scale correction. The curves are the best fit to equation (25) which correspond to fast kinetic regime (FKR) given by equations (22) and (23). The data have been extracted from figure 10.

Table 1
Parameters calculated from data deconvolution ploted in figure. 10. The FKR model allows us to calculate the specific interfacial area of the gas-liquid reactor. The coefficient A calculated in the table is given by equation (23).

$[O_3]_g$ (g m^{-3})	$C^*_{O_3}(M)$	B (abs.units)	t_c (s)	$[BI]_0$ (M)	A (M$^{1/2}$ s^{-1})
3.3	1.64×10^{-5}	1.345 ± 0.005	80.7 ± 0.8	1.08×10^{-4}	1.29×10^{-4}
1.5	7.49×10^{-6}	1.322 ± 0.006	116 ± 1	1.05×10^{-4}	8.82×10^{-5}

table 1. Once A has been calculated, a plot of this parameter against the concentration of the ozone in the gas phase leads to a line passing through the origin. The diffusion coefficient of the ozone in water was set to 1.74×10^{-5} cm^2 s^{-1} [27,28]. The value of the second-order reaction rate constant used was 9.4×10^7 M^{-1} s^{-1} measured at 293 K [29]. The slope of the fit of A against the ozone-gas concentration gives a value of the specific interfacial area of 21 m^{-1}. This value is twice the value predicted using the Akita–Yoshida equation [24] but considering the discrepancies between both experimental methods it can be concluded that the calculated value is in the same order of magnitude of what is expected for the used reactor.

Because the reaction between the ozone and the Blue Indigo is fast enough, the data match FKR model. Some discrepancy at the beginning of the curve (see figure 11) is observed. This phenomenon could be the consequence of the fact that initially the hydrodynamic steady state of the reactor is not achieved or that there is some dispersion process in the gas phase. As it was said previously, these results are a first approach to the problem and a more detailed analysis of data will be needed in the future.

5. Conclusions

The macrotransport transfer function defined in this work is a useful tool for experimental design and data interpretation. Because of its macroscopic character, it is possible to define a perturbation-to-response relationship for systems where one-dimensional macrotransport dispersion equation (1) is applicable. Not only for the signal convolution, that is, the deduction of the response knowing the perturbation, but also for the deconvolution, the perturbation reconstruction knowing the measured response. In classical flow injection analysis textbooks [10,11] the interpretation of the shape of the read response is based on the direct solution of the differential equation (1). The use of some macroscopic models such as the tank-in-series model or the statistical description of the curves calculating the nth moment of the concentration-time curve (see equation (19)) are similar methods to the procedure proposed here, but the advantage of the transfer function is that it allows us to generalise the mathematical treatment to obtain the response of more complex systems, i.e., time varying perturbations, the existence of mixing chambers or chemical reactions. The defined transfer function (2) is a two-parameters function which should be evaluated experimentally. This description seems appropriate because the dispersion parameters, α and β, are related to a microscopic property of the solute such as its diffusion coefficient and because these parameters are also related to the statistical description of the response.

However, a thorough study of the transfer function will be necessary in the future in order to establish an experimental procedure for an accurate determination of the diffusion coefficients, which is a relevant information in the study of gas–liquid reactions. The classical instrumentation for FIA is adequately developed to provide the elements, i.e., pumps, tubes, fittings and flow cells, for this purpose. The fluid velocity ensures that the Poiseuille flow regime applies in most cases and usual tube lengths ensure the usefulness of Aris–Taylor theory. But a detailed analysis of the effect of fluid velocity and tube length on the calculated dispersion parameters would be necessary to confirm experimentally the theory or its limits.

The deconvolution of the response using the transfer function to obtain the perturbation at the tube inlet was also demonstrated. Regularisation is a powerful algorithm which provides a stable solution unconstrained to the hypothesis made about the feasible solution. The procedure presented in this work is limited to systems where no chemical reactions occur along the dispersion tube. So, gas–liquid reactions with fast kinetics are appropriate systems to be analysed by this methodology. On the other hand, detailed description of gas–liquid processes would be necessary. Note that the method proposed here is a way to convert the raw experimental data to the true temporal evolution of the substances in the reactor. In processes completed in few minutes, the method allows us to obtain a high enough number of data to be processed afterwards.

A preliminary analysis of the experimental data about the reaction between the ozone and the Blue Indigo agree with FKR model. The use of flow analysis deconvolution for the determination of the specific area of our gas–liquid reactor has been shown.

Acknowledgments

The authors acknowledge the Generalitat Valenciana for the partial financial support for this project (Ref GV04B-747).

References

[1] H. Brenner and D.A. Edwards, *Macrotransport Processes* (Butterworth-Heineman, Stoneham, 1993).
[2] G. Taylor, Proc. Royal Soc. London, Series A: Mat. Phys. Sci. 219 (1953) 186–203.
[3] G. Taylor, Proc. Royal Soc. London, Series A: Mat. Phys. Sci. 225 (1954) 473–477.
[4] R. Aris, Proc. Royal Soc. London, Series A: Mat. Phys. Sci. 235 (1956) 67–77.
[5] A. Abad et al., *Proceedings of the 15th International Congress of Chemical and Process Engineering*, Prague 2002, Czech Republic.
[6] K. Michielsen, A. Abad, S.C. Cardona, F. López, J.I. Torregrosa, and J. Navarro-Laboulais, *Proceedings of the IOA International Conference (EA3G)*, 2004, Barcelona.
[7] J.J. DiStefano, A.R. Stubberud, and I.J. Williams, *Feedback and Control Systems, 2nd ed.* (Schaum's Outline Series, New York,1990).
[8] D.E. Seborg, T.F. Edgar, and D.A. Mellichamp, *Process Dynamics and Control* (Wiley, New York, 1989).
[9] D. Zwillinger, *CRC Standard Mathematical Tables and Formulae, 30th ed.* (CRC Press, Boca Raton,1996).
[10] B. Kalberg and G.E. Pacey, *Flow Injection Analysis. A Practical Guide* (Elsevier, Amsterdam, 1989).
[11] J. Ruzicka and E.H. Hansen, *Flow Injection Analysis, 2nd ed.* (Wiley, New York, 1988).
[12] L.M. Delves and J.L. Mohamed, *Computational Methods for Integral Equations* (Cambridge University Press, Cambridge, 1985).
[13] Y. Kim and P.A. Nelson, J. Sound Vib. 275 (2004) 463–487.
[14] A. Höcker and V. Kartvelishvili, Nucl. Instr. Meth. A 372 (1996) 469–481.
[15] F. Dion and A. Lasia, J. Electroanal. Chem. 475 (1999) 28–37.
[16] M.E. Orazem, P. Shukla, and M.A. Membrino, Electrochim Acta 47 (2002) 2027–2034.
[17] N. Wu, *The Maximum Entropy Method* (Springer-Verlag, Heidelberg, 1997).
[18] C. Hansen, *Rank-Deficient and Discrete Ill-Posed Problems* (SIAM, Philadelphia, 1998).
[19] A.N. Tikhonov and V.Y. Arsenin, *Solutions of Ill-Posed Problems* (Wiley, Washington, 1977).
[20] A. Alizadeh, C.A. Nieto de Castro, and W. A. Wakeham, Int. J. Thermophysics 1 (1980) 243–284.
[21] F.J. Beltrán, *Ozone Reaction Kinetics for Water and Wastewater Systems* (Lewis Pub., Boca Raton, 2004).
[22] H. Benbelkacem and H. Debellefontaine , Chem. Eng. Process. 42 (2003) 723–732.
[23] F.J. Benitez et al., Chem. Eng. Comm. 119 (1993) 151–165.
[24] W.D. Deckwer, *Bubble Column Reactors* (Wiley, Chichester, 1992).
[25] H. Benbelkacem, S. Mathé and H. Debellefontaine, Water Sci. Tech. 49 (2004) 25–30.
[26] C. Hansen and D.P. O'Leary, SIAM J. Sci. Comput. 14 (1993) 1487–1503.

[27] C.D. Johnson and R.A. Davis, J. Chem. Eng. Data 41 (1996) 1485–1487.
[28] M. Roustan et al., Ozone Sci. Tech. 9 (1987) 289–298.
[29] F. Muñoz and C. von Sontag, J. Chem. Soc. Perkins Trans. 2 2 (2000) 661–664.